Undercompressive Shocks and Riemann Problems for Scalar Conservation Laws with Nonconvex Fluxes

Brian Hayes

Department of Mathematics
Duke University
Durham, NC 27708-0320

and

Michael Shearer[1]

Center for Research in Scientific Computation
and
Department of Mathematics
North Carolina State University
Raleigh, NC 27695–8205

March 22, 1999

ABSTRACT

The Riemann initial value problem is studied for scalar conservation laws whose fluxes have a single inflection point. For a regularization consisting of balanced diffusive and dispersive terms, the traveling wave criterion is used to select admissible shocks. In some cases, the Riemann problem solution contains an undercompressive shock. The analysis is illustrated by exploring parameter space for the Buckley-Leverett flux. The boundary of the set of parameters for which there is a physical solution of the Riemann problem for all data is computed. Within the region of acceptable parameters, the solution has several different forms, depending on the initial data; the different forms are illustrated by numerical computations. Qualitatively similar behavior is observed in Lax-Wendroff approximations of solutions of the Buckley-Leverett equation with no dissipation or dispersion.

---

[1]Adjunct Professor of Mathematics at Duke University. Research supported by National Science Foundation grant DMS 9504583, and by Army Research Office grant DAAH04-94-G-0043.

1 Introduction

We consider a scalar conservation law with nonconvex flux f:

$$u_t + f(u)_x = 0, \tag{1.1}$$

in which $f''(u)$ changes sign at a single inflection point $u = u_I$. The focus of the paper is on the role of undercompressive shock waves in solving Riemann problems for equation (1.1). A Riemann problem is a prototypical initial value problem in which the initial data is piecewise constant with a single discontinuity. An *undercompressive* shock is a discontinuous weak solution of (1.1) with the property that characteristics pass through the shock (as opposed to impinging on the discontinuity from both sides in a *compressive* shock.) It is well known that in order for initial value problems to have unique solutions, additional conditions have to be placed on discontinuous solutions.

In this paper, we study the *traveling wave criterion* for admissibility of shocks, in the context of a regularization of equation (1.1) with both dissipative and dispersive terms. Specifically, a shock wave will be considered to be *admissible* if and only if it is the limit as $\epsilon \longrightarrow 0$ of travelling wave solutions of the equation

$$u_t + f(u)_x = \epsilon\alpha u_{xx} - \epsilon^2\beta u_{xxx}. \tag{1.2}$$

In this equation, the parameters $\alpha \geq 0$ and β will be used to express the relative strengths of dissipation and dispersion. As we shall see below, one sign of β in (1.2) gives undercompressive shocks, the other sign does not. In general, the notion of admissibility depends upon α and β. Similar criteria involving both dissipation and dispersion have been studied for certain scalar equations, hyperbolic systems and systems of mixed type [4, 7, 6, 11, 13, 14, 15].

In the special case that f is a cubic function, undercompressive shocks and their travelling waves can be calculated explicitly, and the solution of the Riemann problem completely analyzed [7]. For a general flux, however, explicit calculations are not available. In Section 4, we characterize the presence of undercompressive shocks by analyzing a parameterized family of vector fields in the plane. Our primary tool is the Melnikov integral [3], related to the the separation (or distance) between the unstable manifold of one equilibrium and the stable manifold of a second equilibrium.

In Section 5, we construct solutions of the Riemann problem. Broadly, the results are similar to the case of a cubic flux. In particular, for some initial data, the solution has two waves. When the two waves are shocks, specifically a compressive shock and an undercompressive shock, the solution $u(x,t)$ is nonmonotone as a function of x for fixed t. The results are formulated for equations (like the Buckley–Leverett equation) in which f maps the interval $[0,1]$ into itself, and $0 < u_I < 1$. Because the solution may be nonmonotonic, it follows that for some data in $[0,1]$, the solution of the Riemann problem may take values outside the unit interval, i.e., outside the physical domain. We formulate sufficient conditions on flux functions f, and the range of parameters α, β

under which the unit interval is invariant under solving the Riemann problem. The results are illustrated for the one-parameter family of fluxes given by

$$f(u;a) = \frac{u^2}{u^2 + a(1-u)^2}. \tag{1.3}$$

Specifically, with $\alpha = \theta, \beta = 1-\theta, \quad 0 \le \theta \le 1$, we calculate (numerically) the boundary in (a, θ) between equations for which the Riemann problem is solvable in $[0,1]$ and those for which the Riemann problem is not solvable in $[0,1]$ for some initial data in the interval.

In Section 6, we show numerical results of finite difference approximations that illustrate the structure of solutions of Riemann problems that we have established theoretically.

2 Rarefactions and Shocks

Recall that the characteristic speed of equation (1.1) is $f'(u)$. A *centered rarefaction wave* is a continuous piecewise smooth weak solution of (1.1) that has the scale invariant form

$$u(x,t) = \begin{cases} u_- & \text{if} \quad x \le f'(u_-)t \\ \\ \overline{u} & \text{if} \quad f'(u_-)t \le x = f'(\overline{u})t \le f'(u_+)t \\ \\ u_+ & \text{if} \quad x \ge f'(u_+)t. \end{cases} \tag{2.1}$$

A *centered shock wave*

$$u(x,t) = \begin{cases} u_- & \text{if} \quad x < st \\ \\ u_+ & \text{if} \quad x > st. \end{cases} \tag{2.2}$$

with speed s is a weak solution of (1.2) if the triple (u_-, u_+, s) satisfies the Rankine-Hugoniot condition

$$-s(u_+ - u_-) + f(u_+) - f(u_-) = 0. \tag{2.3}$$

Thus the shock speed

$$s = \left(f(u_+) - f(u_-)\right) / (u_+ - u_-) \tag{2.4}$$

is the slope of the chord joining the points $(u_\pm, f(u_\pm))$ in the graph of f.

A shock (2.2) is called *compressive,* or a *Lax shock* if it satisfies the Lax entropy condition [8], which relates the slope of the chord, given by (2.4), to slopes of f:

$$f'(u_+) \le s \le f'(u_-). \tag{2.5}$$

For a function f having at most one inflection point, it easy to show that the Lax entropy condition is equivalent, for centered shock waves (2.2), to the entropy condition (E) of Oleinik [10] and to the viscosity criterion, involving the existence of smooth travelling wave solutions of (1.2) with $\beta = 0$ (i.e., including viscosity, or dissipation, but not dispersion).

A *rarefaction–shock* is a combination of a rarefaction wave and a shock wave, in which the fastest characteristic in the rarefaction wave, $x = f'(u_o)t$, is also the shock: $x = st, s = f'(u_o) = (f(u_+) - f(u_o))/(u_+ - u_o)$.

3 Travelling Waves and Lax Shocks

To describe shock waves (2.2) admissible under the traveling wave criterion with $\beta \neq 0$, we consider travelling wave solutions $u = u(\xi), \xi = (x - st)/\epsilon$ of (1.2) with the boundary conditions

$$u(\pm\infty) = u_\pm, \quad u'(\pm\infty) = 0 = u''(\pm\infty). \tag{3.1}$$

Substituting into equation (1.2) and integrating from $\xi = -\infty$, we obtain the ordinary differential equation

$$\beta u'' = \alpha u' - (f(u) - f(u_-) - s(u - u_-)). \tag{3.2}$$

This second-order equation is equivalent to the first-order system

$$\begin{array}{rl} u' & = v \\ \beta v' & = \alpha v - (f(u) - f(u_-) - s(u - u_-)). \end{array} \tag{3.3}$$

Equilibria of (3.3) are of the form $(u, v = 0)$, with

$$f(u) - f(u_-) - s(u - u_-) = 0. \tag{3.4}$$

If $(u_+, 0)$ is an equilibrium, then the Rankine Hugoniot condition (2.3) holds, so that the triple (u_-, u_+, s) represents a shock wave solution (2.2) of the hyperbolic equation (1.1).

To simplify the description of Lax shocks, we distinguish those fluxes for which $f''(u)$ and $u - u_I$ have the same sign from the rest, by the expedient of assuming that $f'''(u) \neq 0$ for all u. Consider a chord through u_-, with slope s, that intersects the graph of f at three places, the value of u at each intersection corresponding to an equilibrium $(u, 0)$. We shall distinguish between the *outside equilibria* corresponding to the largest and smallest values of u, and the *middle equilibrium*, corresponding to the middle value of u. We then have the following characterization of the equilibria, depending on the signs of β and f''' :

A. If $\beta f''' < 0$, then the outside equilibria are saddle points, and the middle equilibrium is a node, stable if $\beta > 0$ and unstable if $\beta < 0$.

B. If $\beta f''' > 0$, then the outside equilibria are nodes, stable if $\beta > 0$ and unstable if $\beta < 0$; the middle equilibrium is a saddle point.

We easily see that Lax shocks, corresponding to triples (u_-, u_+, s) satisfying (2.3) and (2.5), have the following characterization:

If $\beta > 0$, then $(u_-, 0)$ is a saddle and $(u_+, 0)$ is a stable node;

If $\beta < 0$, then $(u_-, 0)$ is an unstable node and $(u_+, 0)$ is a saddle.

Putting these observations together with a simple consideration of the phase plane for system (3.3) leads to the following.

Lemma 3.1 *If $\beta f''' > 0$, then all Lax shocks are admissible, and conversely, all admissible shocks satisfy the Lax entropy condition.*

On the other hand, if $\beta f''' < 0$, then there are admissible shocks that are not Lax shocks, and some Lax shocks are not admissible. The complete characterization of this structure is given in the next section, but we have the following partial result paralleling Lemma 3.1:

Lemma 3.2 *If $\beta f''' < 0$, and (u_-, u_+, s) is a Lax shock such that u_-, u_+ are on the same side of u_I, then the shock is admissible.*

4 Undercompressive Shocks

In this section, we analyze the vector field (3.3) in the Case **A** above. For definiteness, and with the Buckley-Leverett equation in mind, we henceforth assume that

$$f''(u) > 0 \quad \text{for} \quad u < u_I, \quad \text{and} \quad f''(u) < 0 \quad \text{for} \quad u > u_I, \tag{4.1}$$

and consider $\beta > 0$. It is convenient to combine $\alpha > 0$ and $\beta > 0$ into a single variable $\gamma = \alpha/\sqrt{\beta}$. After rescaling variables, we obtain the system

$$\begin{aligned} u' &= v \\ v' &= \gamma v - (f(u) - f(u_-) - s(u - u_-)). \end{aligned} \tag{4.2}$$

If u_- and u_+ are saddle point equilibria for (3.3), and there is a heteroclinic orbit from $(u_-, 0)$ to $(u_+, 0)$ in the phase plane, then we say $u_- \longrightarrow u_+$ is a *saddle-to-saddle connection.* In particular, (2.2) is an undercompressive shock if and only if the Rankine Hugoniot condition (2.3) is satisfied and $u_- \longrightarrow u_+$ is a saddle-to-saddle connection.

Let $u_- < u_I$. We restrict attention to the range of s for which $(u_-, 0)$ is the leftmost saddle point: $s > f'(u_-)$. At least near $(u_-, 0)$, the unstable manifold is a curve in the

phase plane that can be parameterized by u. Let $v = v(u)$ along the unstable manifold through $(u_-, 0)$. We have the following relation,

$$\frac{1}{2}(v(u))^2 = \gamma \int_{u_-}^{u_+} v(y)\, dy - \int_{u_-}^{u_+} (f(y) - f(u_-) - s(y - u_-))\, dy. \tag{4.3}$$

In particular, if (u_-, u_+, s) corresponds to an undercompressive shock, then it is straightforward to check that the trajectory joining $(u_-, 0)$ to $(u_+, 0)$ is the graph of v over the interval $[u_-, u_+]$, and since $v(u) > 0, \gamma > 0$, we have from $v(u_+) = 0$ and (4.3) that

$$\int_{u_-}^{u_+} (f(y) - f(u_-) - s(y - u_-))\, dy > 0 \tag{4.4}$$

That is, if $u_- \longrightarrow u_+$ is a saddle-to-saddle connection then the signed area between the graph of f and the chord with slope s intersecting the graph at $u = u_\pm$ must be positive.

Let $s = s_E(u_-)$ be the unique value of s for which the signed area is zero:

$$\int_{u_-}^{u_E} f(y)\, dy = (f(u_E) + f(u_-))(u_E - u_-); \quad s_E(u_-) = (f(u_E) - f(u_-))/(u_E - u_-). \tag{4.5}$$

Then (4.4) implies that the range of values of s for which there can be a saddle-to-saddle connection from u_- to some u_+ is

$$f'(u_-) < s < s_E(u_-). \tag{4.6}$$

In this section, we prove the following theorem. The theorem is illustrated in Figure 1.

Theorem 4.1 *Let $\gamma = \gamma^o > 0$, and suppose that there is a saddle-to-saddle connection $u_-^o \longrightarrow u_+^o$ for some $u_-^o < u_I < u_+^o$. Then for each $\gamma > 0$ near γ^o, there is $u^* = u^*(\gamma) < u_I$ and a C^1 function $g(u_-), u_- < u^*$ such that:*

(a) $u_- \longrightarrow u_+$ is a saddle-to-saddle connection with s in the range (4.6) if and only if $s = g(u_-) = (f(u_+) - f(u_-))/(u_+ - u_-)$ and $u_- < u^*$;

(b) $\dfrac{dg}{du_-}(u_-) > 0$ for $u_- < u^*$;

(c) writing $u_+ = u_+(u_-)$, we have $\dfrac{du_+}{du_-}(u_-) < 0$ for $u_- < u^*$;

(d) $\lim_{u_- \longrightarrow u^*-} g(u_-) = f'(u^*)$.

Proof The proof centers on an analysis of the separation between the unstable manifold from one saddle point equilibrium and the stable manifold of a second saddle point equilibrium. To set this up, we introduce some simplifying notation.

Write μ for the triple of parameters in the vector field of (4.2): $\mu = (s, u_-, \gamma)$. We shall use a superscript zero to indicate quantities evaluated at a specific value (s^o, u_-^o, γ^o).

Thus, $\mu^o = (s^o, u_-^o, \gamma^o)$. Similarly, we let $\phi = (u, v)$, and we let $H(\phi; \mu)$ denote the vector field in (4.2), so that

$$H(\phi;\mu) = \begin{pmatrix} v \\ \gamma v - (f(u) - f(u_-) - s(u - u_-)) \end{pmatrix} \tag{4.7}$$

Let $dH/d\phi$ denote the Jacobian matrix of H with respect to $\phi = (u, v)$. Then

$$\mathrm{div} H = \gamma \tag{4.8}$$

is the divergence of H with respect to ϕ, i.e., the trace of $dH/d\phi$.

For a specific $\gamma^o > 0$, consider a saddle-to-saddle connection $u_-^o \longrightarrow u_+^o$ with speed s^o. Let $\phi^o(\xi) = (u^o(\xi), v^o(\xi))$ be the corresponding trajectory, a solution of (4.2) with $\phi^o(\pm\infty) = (u_\pm^o, 0)$. For μ near μ^o, there are corresponding saddle points $(u_\pm, 0)$ near $(u_\pm^o, 0)$ respectively. Let $\phi_-(\xi;\mu)$ be a solution of (4.2) along the unstable manifold of $(u_-, 0)$ such that ϕ_- is C^1 in (ξ, μ) for μ in a neighborhood of μ^o and $-\infty < \xi \le 0$, with $\phi_-(\xi;\mu^o) = \phi^o(\xi),\ -\infty < \xi \le 0,\ \phi_-(-\infty;\mu) = (u_-, 0)$. Similarly, let $\phi_+(\xi;\mu),\ 0 \le \xi < \infty$ be a solution of (4.2) along the stable manifold of $(u_+, 0)$.

Let $y(\xi) = H(\phi_-(\xi,\mu),\mu) \wedge \partial_\theta \phi_-(\xi,\mu)$, where $\wedge$ denotes the determinant with columns given by the vectors on either side, or the vector product between vectors in two dimensions, and θ is one of the parameters s, u_-, γ. Then a simple calculation establishes that y satisfies the linear differential equation

$$\frac{dy}{d\xi} = a(\xi)\, y + r(\xi), \tag{4.9}$$

where

$$a(\xi) = \mathrm{div} H(\phi_-(\xi,\mu),\mu) = \gamma, \quad \text{and} \quad r(\xi) = H(\phi_-(\xi,\mu),\mu) \wedge \frac{\partial H(\phi_-(\xi,\mu),\mu)}{\partial \theta}.$$

In particular, integrating this equation from $\xi = -\infty$ to $\xi = 0$, and using the boundary condition $H = 0$ at $\xi = -\infty$, we obtain

$$y(0) = \int_{-\infty}^{0} K(\xi) r(\xi)\, d\xi, \tag{4.10}$$

where $K(\xi) = exp(-\int_0^\xi a(\zeta)\, d\zeta) = e^{-\gamma\xi}$. Thus, if we define the *separation function* R by

$$R(\mu) = H(\phi^o(\xi),\mu^o) \wedge (\phi_-(0;\mu) - \phi_+(0;\mu)), \tag{4.11}$$

then

$$\frac{\partial R}{\partial \theta}(\mu^o) = \int_{-\infty}^{\infty} K(\xi) \left(H(\phi^o(\xi),\mu^o) \wedge \frac{\partial H}{\partial \theta}(\phi^o(\xi),\mu^o) \right) d\xi. \tag{4.12}$$

This formula is the Melnikov integral commonly used to analyze separation functions between manifolds for the Poincare map of a dynamical system [3]. Here, the application

is perhaps simpler, and the form of H makes the analysis particularly simple. From formula (4.12), we calculate

$$\frac{\partial R}{\partial s}(\mu^o) = \int_{-\infty}^{\infty} e^{-\gamma\xi} v^o(\xi)(u^o(\xi) - u_-^o)\, d\xi > 0, \qquad (a)$$

$$\frac{\partial R}{\partial u_-}(\mu^o) = \int_{-\infty}^{\infty} e^{-\gamma\xi} v^o(\xi)(f'(u_-^o) - s^o)\, d\xi < 0, \qquad (b) \qquad (4.13)$$

$$\frac{\partial R}{\partial \gamma}(\mu^o) = \int_{-\infty}^{\infty} e^{-\gamma\xi} v^o(\xi)^2\, d\xi > 0. \qquad (c)$$

In particular, from (4.13a), we have that locally, the speed s of a saddle-to-saddle connection is a function of u_- and $\gamma : s = \hat{s}(u_-, \gamma)$, and

$$R(\hat{s}(u_-, \gamma), u_-, \gamma) = 0. \qquad (4.14)$$

Moreover, from the Rankine-Hugoniot condition (2.3), since $f'(u_+) - s < 0$, we have that u_+ is a function of u_- and s, so that the value of u_+ for a saddle-to-saddle connection depends on γ only through $\hat{s}$, say $\hat{u}_+(u_-, \gamma) = u_+(\hat{s}(u_-, \gamma), u_-)$. From the Rankine Hugoniot condition (2.3), we find

$$\frac{\partial u_+}{\partial s} = \frac{u_+ - u_-}{f'(u_+) - s} < 0; \qquad \frac{\partial u_+}{\partial u_-} = \frac{f'(u_-) - s}{f'(u_+) - s} > 0. \qquad (4.15)$$

From (4.13), (4.14), we have that

$$\frac{\partial \hat{s}}{\partial \gamma} = -R_\gamma / R_s < 0, \qquad \frac{\partial \hat{s}}{\partial u_-} = -R_{u_-} / R_s > 0, \qquad (4.16)$$

so that, using (4.15),

$$\frac{\partial \hat{u}_+}{\partial \gamma} = \frac{\partial u_+}{\partial s}\frac{\partial \hat{s}}{\partial \gamma} > 0. \qquad (4.17)$$

Similarly,

$$\frac{\partial \hat{u}_+}{\partial u_-} = \frac{\partial u_+}{\partial u_-} + \frac{\partial u_+}{\partial s}\frac{\partial \hat{s}}{\partial u_-}, \qquad (4.18)$$

but the first term on the right hand side is positive while the product is negative, so to determine the sign in (4.18), we use more information from the Melnikov integral. Specifically, from (4.13) and (4.18), we get

$$\frac{\partial \hat{u}_+}{\partial u_-} = \left(\frac{f'(u_-^o) - s}{f'(u_+^o) - s}\right)\left(1 - (u_+^o - u_-^o)\frac{\int_{-\infty}^{\infty} e^{-\gamma\xi} v^o(\xi)\, d\xi}{\int_{-\infty}^{\infty} e^{-\gamma\xi} v^o(\xi)(u^o(\xi) - u_-^o)\, d\xi}\right). \qquad (4.19)$$

The first factor on the right hand side is positive since $s > f'(u_\pm^o)$; the second factor is negative by virtue of the facts that $u^o(\xi) < u_+^o$ for $-\infty < \xi < \infty$, and $u_+^o > u_-^o$. Thus,

$$\frac{\partial \hat{u}_+}{\partial u_-} < 0. \qquad (4.20)$$

For fixed $\gamma > 0$, the intersection of the curve $s = \hat{s}(u_-, \gamma)$ with the curve $s = f'(u_-)$ represents a singularity in the family of vector fields at which a saddle-node equilibrium (at $(u^*, 0)$) is connected in the phase plane by a special separatrix to the corresponding saddle point $(u_+, 0)$. Such a separatrix-saddle-node singularity can be handled via the Melnikov integral by parameterizing the vector fields by u_- and u_+, eliminating s [12, 13]. Then u_+ is found as a decreasing function of u_-; s is increasing in u_-. For $u_- < u^*$, $u_- \longrightarrow u_+$ is a saddle-to-saddle connection; for $u^* < u_-$, $u_- \longrightarrow u_+$ is a distinguished node-to-saddle heteroclinic orbit. The phase portraits near the singular vector field are as shown in Figure 1. We omit the details of this calculation.

The dependence of the sign of the separation function $R(s, u_-, \gamma)$ upon the parameters near a zero of R is of course determined by the formulae (4.13). In particular, the sign of $\partial R/\partial s$ implies that for fixed $\gamma > 0$, for each u_- and each s in the interval (4.6), there is at most one s for which the vector field has a saddle-to-saddle connection. Thus, the set SS of such pairs (u_-, s) is indeed a single curve, as shown in Figure 1, and described in the Theorem. This completes the proof.

Remark. It is easy to perturb away from the case $\gamma = 0$, for which the saddle-to-saddle connections satisfy the equal area rule (i.e., the signed area in (4.4) is zero when there is a saddle-to-saddle connection $u_- \longrightarrow u_+$, so that $\hat{s}(u_-, 0) = s_E(y_-)$ given by (4.5)). Such a perturbation establishes the picture of parameter space shown in Figure 1. The behavior for general γ follows by noting that the only possible singularity is for u^* to become infinite. This possibility could be avoided by making suitable assumptions on f, but we do not pursue this technical point here, and instead proceed under the assumption that $u^*(\gamma)$ is finite, and we may take Figure 1 to accurately portray the phase portraits for all values of s and u_- of interest, for any fixed γ. In the figure, values of the parameters for which the vector field is structurally stable are denoted *P1* and *P2*. The curves are labeled according to their special roles. Thus, the upper curve correspond to the equal area rule, for which $s = s_E(u_-)$; the curve labeled SS corresponds to vector fields with a saddle-to-saddle connection while those labeled SN1 and SN2 correspond to the degenerate vector fields in which a saddle point and a node have merged at u_-.

5 The Riemann Problem

The Riemann problem is the initial value problem

$$\begin{aligned} u_t + f(u)_x &= 0 \\ u(x,0) &= \begin{cases} u_L & \text{if} \quad x < 0 \\ u_R & \text{if} \quad x > 0. \end{cases} \end{aligned} \tag{5.1}$$

As in Section 4, we assume $f''(u)(u - u_I) < 0$ for $u \neq u_I$.

In the classical setting of Lax and Oleinik [8, 10], for which shocks are admissible if and only if they are compressive, the Riemann problem has a unique admissible solution

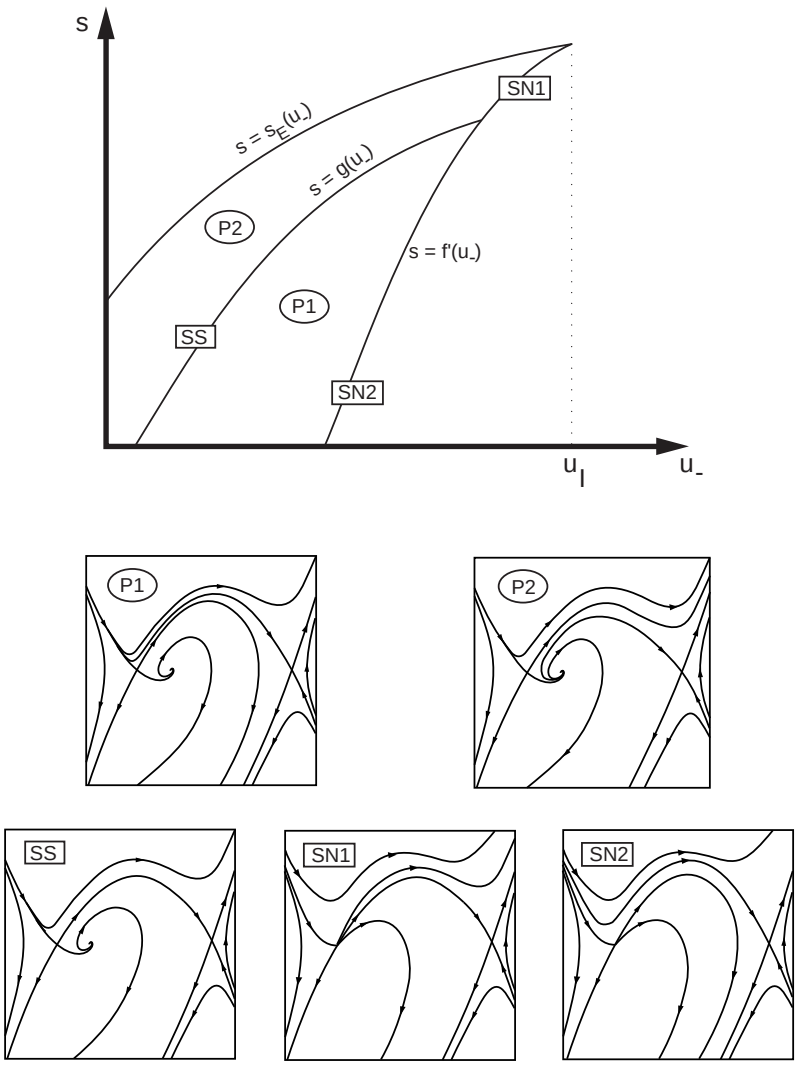

Figure 1: *Phase Portraits.*

for all initial data. The solution has a very simple dependence on the data. Consider $u_L < u_I$. The solution consists of constant states u_L, u_R, separated in the (x,t)–plane by a single wave. Let u_L^T be the point for which $f'(u_L) = (f(u_L^T) - f(u_L))/(u_L^T - u_L)$, if such a point exists; otherwise, let $u_L^T = \infty$. Then the single wave is:

A shock if $u_R < u_L$;
A rarefaction wave if $u_L < u_R < u_I$;
A rarefaction–shock if $u_I < u_R < u_L^T$;
A shock if $u_R > u_L^T$.

We refer to this solution as the *classical solution.* A feature of the classical solution $u = u(x/t)$ is that it is monotonic.

When some undercompressive shocks are deemed admissible, for example, taking $\beta > 0$ in equation (1.2), then the solution is more complicated. In particular, there may be no admissible solution, while some solutions are not monotonic.

The objective of this section is to show how the classical solution (valid for u_R close to u_L) gives way to a non–classical solution (i.e., with undercompressive shocks) as $|u_R - u_L|$ increases.

However, information from Theorem 1 concerning undercompressive shocks is not enough to characterize the dependence of the solution of the Riemann problem on the data. Additional information is needed about the behavior of the middle equilibrium $u_o(u_-, \gamma)$ when there is a saddle-to-saddle connection $u_- \longrightarrow u_+$. For example, when $f(u) = u^3$ (and $\beta < 0$, to fit into Case A), the middle equilibrium can be explicitly calculated, and is found to be independent of u_- [7]. Perturbing away from this special case could give various types of dependence of u_o on u_-. The dependence of the solution of the Riemann problem on the behavior of u_o is subtle. Rather than attempt an exhaustive catalog of possible solutions, we construct solutions under specific conditions on the flux and the behavior of the middle equilibrium.

5.1 Buckley-Leverett Fluxes.

The Buckley-Leverett equation is a model for the flow of two immiscible fluids in a porous medium. Let u and $1-u$ denote the volume fractions of the two fluids in the pore volume, and let $k_1(u), k_2(1-u)$ be the relative permeabilities, divided by viscosity, of the medium to the fluids. Typically, these functions are monotonically increasing and convex:

$$k_j(0) = 0 = k_j'(0); \quad k_j''(w) > 0, \quad 0 \le w \le 1; \quad k_j(1) = 1/\mu_j, \quad j = 1, 2, \tag{5.2}$$

where μ_1, μ_2 are the viscosities of the fluids.

The Buckley Leverett equation that we consider includes an additional dispersive term:

$$u_t + f(u)_x = \epsilon u_{xx} - \epsilon^2 \gamma u_{xxx}, \tag{5.3}$$

where

$$f(u) = \frac{k_1(u)}{k_1(u) + k_2(1-u)}, \quad 0 \le u \le 1, \tag{5.4}$$

and $0 \le \theta \le 1$.

We remark that the dissipative term ϵu_{xx} in (5.3) is generally referred to as *dispersion* in the literature on two phase flow in porous media [1]. The (mathematically) dispersive term $-\epsilon^2 \gamma u_{xxx}$ is not usually included in the model equations. This term may be part of the truncation error of a numerical method. The connection between numerical methods for scalar conservation laws with non-convex fluxes, dispersive terms in the corresponding truncation errors, and the appearance of undercompressive shocks in simulations is explored in [4].

From the properties (5.2) of the relative permeabilities, it is easily checked that the flux function f is nonconvex in the unit interval. Specifically,

$$f(0) = 0 = f'(0); \quad f(1) = 1; f'(1) = 0; \quad f''(0) > 0; f''(1) < 0. \tag{5.5}$$

In this subsection, we consider the flux f to have the S shape characteristic of the Buckley-Leverett equation. That is, suppose f is C^2, monotonically increasing on the interval $[0, 1]$, and has a single inflection point u_I. As for the Buckley-Leverett equation, we assume f satisfies (5.5).

The dependent variable $u = u(x, t)$ is constrained to lie in the interval $[0, 1]$. For classical solutions of the Riemann problem, this constraint presents no difficulty, because the solution is monotonic. Thus, for initial data in the interval, the solution is also in the interval. But for nonclassical solutions, $u(x, t)$ may be nonmonotonic in x, in particular when the solution involves a combination of undercompressive and compressive shocks. Consequently, there are Buckley-Leverett fluxes, and ranges of initial data,for which there is no non-classical solution of the Riemann problem that remains in the physical domain, even though the classical solution is well defined. Since we wish to find non-classical solutions of the Riemann problem for all initial data in the physical domain, it is necessary to place constraints on the flux. The following two conditions concerning undercompressive shocks implicitly involve the flux function and the balance between dissipation and dispersion.

Assumption I There is $u_1^- \in [0, u_I]$ such that $u_1^- \longrightarrow 1$ is a saddle-to-saddle connection; correspondingly, there is $u_0^- \in [u_I, 1]$ such that $u_0^- \longrightarrow 0$ is a saddle-to-saddle connection.

This assumption is necessary for the Riemann Problem to have a solution for all data, with non-classical solutions for some data. In Subsection 5.2, we investigate the assumption numerically. The second assumption, for which we first introduce some notation, is not important for the *existence* of solutions of the Riemann problem (although we do not offer a proof of existence without the assumption). However, as remarked above, the *structure* of the solutions (which waves are included in, or eliminated from, the solution as the data change) is simplified with this assumption. Let $u_o(u_-)$ be the middle equilibrium of a saddle-to-saddle connection $u_- \longrightarrow u_+$. Then from Theorem 1, and Assumption *I*, there exist u^*, u^{**} such that u_o is defined and continuous on $[u_1^-, u^*] \cup [u^{**}, u_o^-]; u_o(u^*) = u^*, u_o(u^{**}) = u^{**}$.

Assumption II The function u_o is monotonically decreasing from $\overline{u}_1 = u_o(u_1^-)$ to u^*, and from u^{**} to $\overline{u}_o = u_o(u_o^-)$.

With these assumptions, we can solve the Riemann problem for any Riemann data u_L, u_R in $[0, 1]$. For definiteness, we first consider various $u_L < u_I$, and show the solution for all $u_R \in [0, 1]$. We then combine these solutions with solutions for $u_L > u_I$ to

show the division of the (u_L, u_R) plane into different regions corresponding to different combinations of waves in the solution.

To start with, we have several cases depending on the location of u_L :

(i) $\overline{u}_1 < u_L < u_I$. In this case, the solution is *classical*, and is shown in Figure 2. In this figure, depicting the solution for a fixed value of u_L, and for each $u_R \in [0,1]$, the letters R, S indicate solutions consisting of a single shock wave, rarefaction wave, respectively; the designation RS represents a rarefaction–shock wave solution. The transition from rarefaction–shock solution to a single shock solution occurs at $u_R = u_L^T$, defined to be the value of u_R for which there is a shock from u_L to u_R with speed $f'(u_L)$.

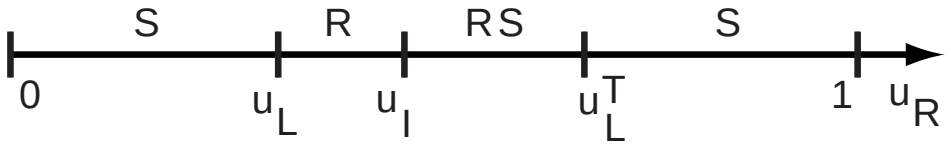

Figure 2: *Solution of the Riemann Problem. Case (i).*

(ii) $u^* < u_L < \overline{u}_1$. By Assumption *II*, there exists a unique u_-, say $u_- = u_L^-$ such that $u_L = u_o(u_L^-)$. Let $\tilde{u}_L = u_+(u_L^-)$ be the right equilibrium. Thus, for $u_R = \tilde{u}_L$, there is a solution of the Riemann problem involving a Lax shock from u_L to u_L^- and an undercompressive shock from u_L^- to u_R. The two shocks have the same speed. This degenerate solution is the limiting case of two distinct solutions, depending on nearby values of u_R. For $u_R < \tilde{u}_L$ (near $\tilde{u}_L$), the uniquely defined undercompressive shock $u_- \longrightarrow u_R$ is slower than the Lax shock joining u_L to u_-, so that the only possible solution is a single admissible Lax shock from u_L to u_R, which becomes inadmissible as u_R crosses $\tilde{u}_L$. For $u_R > \tilde{u}_L$ (near $\tilde{u}_L$), the undercompressive shock is faster than the the Lax shock joining u_L to u_- (this follows by comparing slopes of chords in the graph of f, and from Assumption *I*), so the solution consists of these two shocks; the Lax shock from u_L to u_R is now inadmissible.

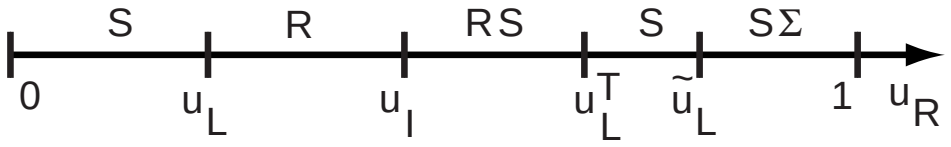

Figure 3: *Solution of the Riemann Problem. Case (ii).*

In Figure 3, we use the notation $S\Sigma$ to indicate the interval of values of u_R for which the solution consists of a Lax shock and a faster undercompressive shock.

(iii) $u_1^- < u_L < u^*$. For u_L in this range, there is a saddle-to-saddle connection from u_L to $u_L^+ = u_+(u_L)$ shown in Figure 4. Perturbing u_R away from u_L^+ gives the rarefaction–

undercompressive shock (in which the shock travels faster than the rarefaction wave, and is detached from it), and Lax shock-undercompressive shock constructions shown in the figure. The transition from rarefaction–shock to rarefaction–undercompressive shock occurs at $u^r = u_+(u^*)$, where the shock in the rarefaction–shock construction first becomes inadmissible.

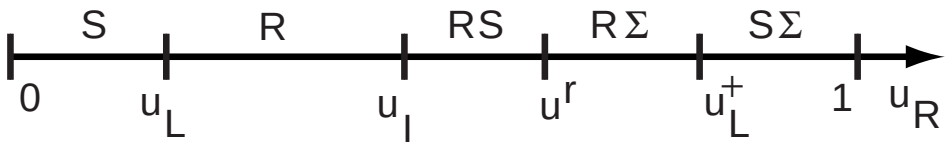

Figure 4: *Solution of the Riemann Problem. Case (iii).*

(iv) $0 < u_L < u_1^-$. Here, u_L is to the left of the domain of the function u_+, so that in order to have a solution with an undercompressive shock, there must first be a rarefaction wave. In particular, the interval of u_R in which there is a shock-undercompressive shock solution collapsed onto $u_r = 1$ as u_L approached u_1^-, and has now disappeared in Figure 5.

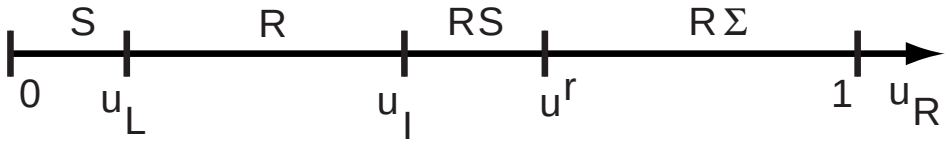

Figure 5: *Solution of the Riemann Problem. Case (iv).*

For $u_L > u_I$, the solution of the Riemann problem is symmetric in the natural way. Since we are discussing solutions of a scalar equation, we can represent solutions in the $u_L - u_R$ plane, shown in Figure 6.

If Assumption *I* fails, then there may be no solution of the Riemann problem for some data. Specifically, suppose there is no saddle-to-saddle connection $u_- \longrightarrow 1$ with $u_- \in [0, u_I)$, and $u^* \in (0,1)$ is such that $u_+(u^*) \in (0,1)$. Consider the Riemann problem with data $u_L = 0, u_R = 1$. Then the classical solution of a rarefaction–shock is inadmissible, while the nonclassical solution must involve an undercompressive shock to $u_R = 1$, which necessarily has a left state outside $[0,1]$. Note that if $u^* \notin (0,1)$, and $u^{**} \notin (0,1)$, then all admissible shocks are Lax shocks.

On the other hand, the failure of Assumption *II* does not affect the solution very much. The solution is still well defined under reasonable conditions (for example, if u_o has a single maximum), but the arrangement of the solution in the $u_L - u_R$ plane is slightly different. Considering the scalar equation on the entire real line introduces further possibilities for the behavior of the solution. For example, if the graph of f has asymptotes of different slopes, then the shock-undercompressive shock solutions can involve extremely large variation in the solution, approaching infinity in limiting cases.

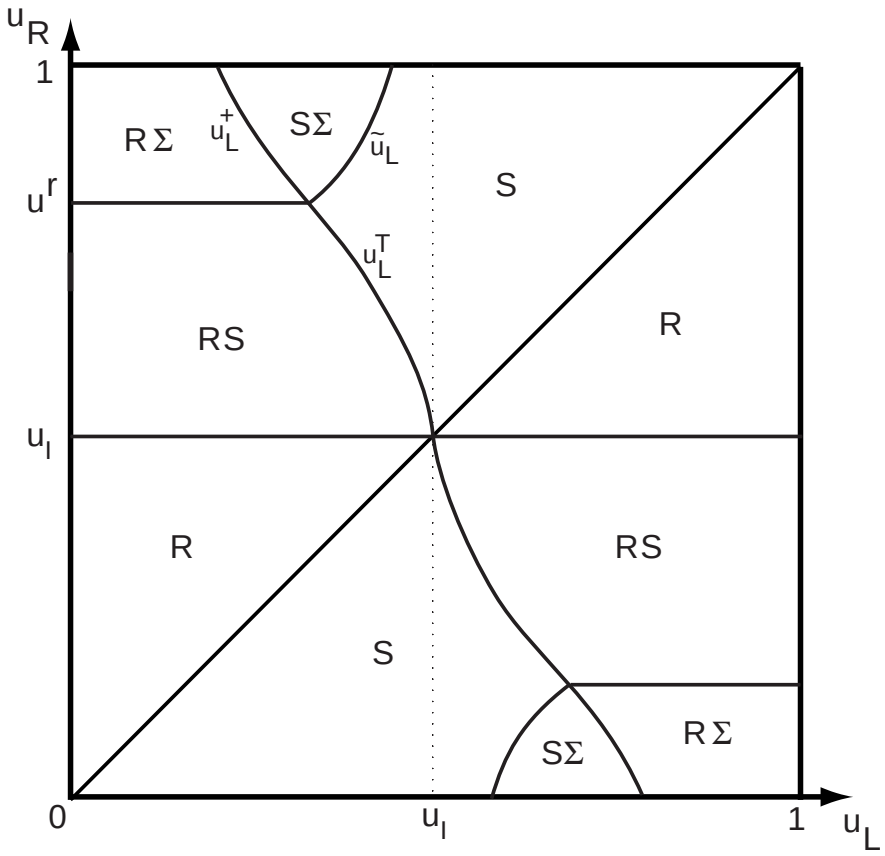

Figure 6: *Solution of the Riemann Problem.*

We show some examples of these somewhat bizarre solutions in the section on numerical results.

5.2 An Example: Quadratic Relative Permeabilities.

The specific Buckley–Leverett equation that we consider is

$$u_t + f(u)_x = \epsilon\theta u_{xx} - \epsilon^2(1-\theta)u_{xxx}, \tag{5.6}$$

where

$$f(u) = \frac{k_1(u)}{k_1(u) + k_2(1-u)}, \quad 0 \le u \le 1, \tag{5.7}$$

and $0 \le \theta \le 1$. The relative permeabilities are taken to be quadratic fundtions:

$$k_1(u) = K_1 u^2, k_2(u) = K_2 u^2,$$

where K_1, K_2 are positive constants. Then

$$f(u) = \frac{K_1 u^2}{K_1 u^2 + K_2(1-u)^2} = \frac{u^2}{u^2 + a(1-u)^2}, \tag{5.8}$$

where $a = K_2/K_1$. The graph of this function f for various values of the parameter a is shown in Figure 7.

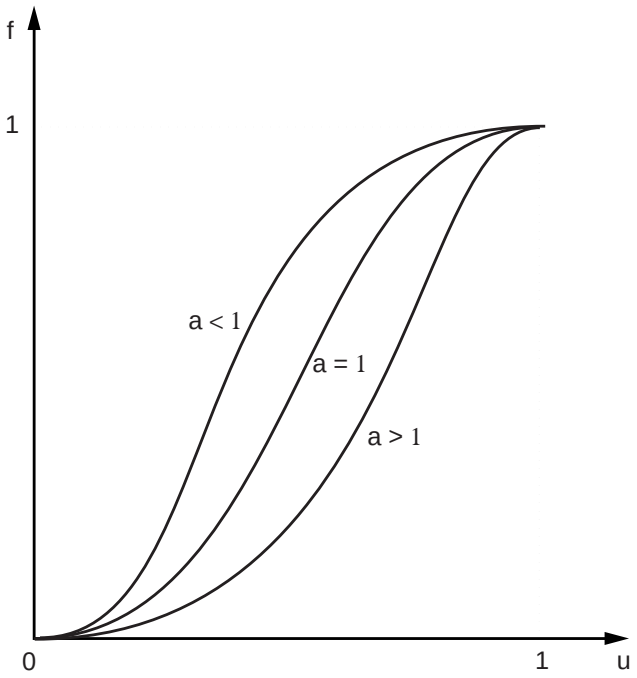

Figure 7: *Buckley-Leverett Fluxes.*

Whether solutions of Riemann problems take values in $[0, 1]$ when the initial data u_L, u_R lie in that interval rests on where the the states on either side of undercompressive shocks take their values. This in turn depends solely on the location of the value of u on one side of an undercompressive shock when the value of u on the other side of the shock is either zero or one, that is, on the boundary of the physically relevant domain for u.

Specifically, we can test Assumption I of the last section. Whether this assumption holds depends on the values of the two parameters θ (balancing dissipation and dispersion), and a, from the flux function (5.8). In Figure 8, we show a curve in this parameter space, separating values for which Assumption I holds (labelled $GOOD$) from those for which the assumption fails (labelled BAD). The curve for $a \leq 1$ is determined from the condition that there is a saddle-to-saddle connection $0 \longrightarrow 1$ (with speed one). For $a \leq 1$, it follows by consideration of the signed area between the chord and the graph of f, that there is a saddle-to-saddle connection $1 \longrightarrow 0$ (also with speed one). The corresponding curve for $a > 1$, is obtained from Figure 8 by the transformation $(a, \theta) \longrightarrow (1/a, \theta)$, corresponding to $u \longrightarrow 1 - u$.

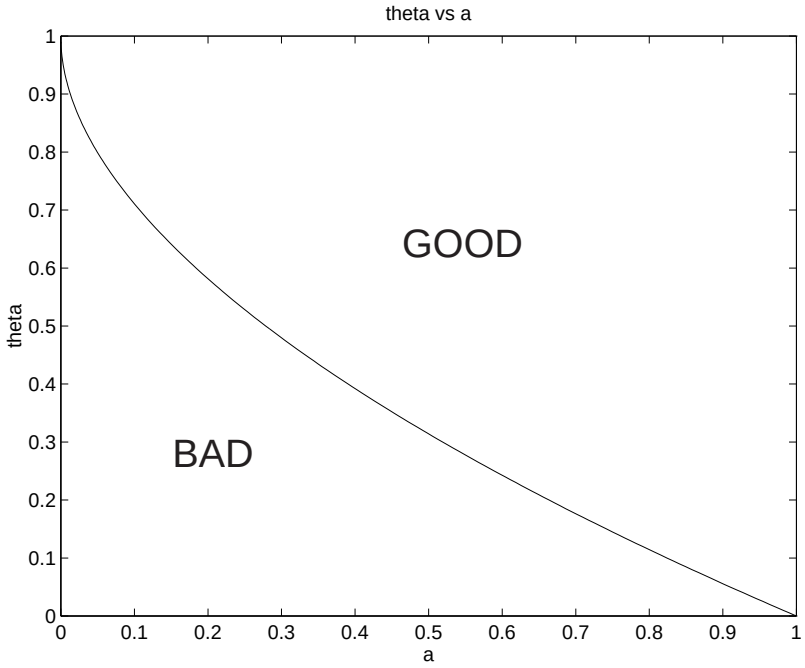

Figure 8: *Assumption I for the Buckley-Leverett equation.*

6 Numerical Results

In this section, we study numerical solutions of non-convex conservation laws with diffusion and dispersion. In the first subsection, we illustrate the theoretical results of the previous section on the Riemann problem for the Buckley-Leverett equation with dispersion. In the second subsection, we consider a different nonconvex flux, and also the effect of a second-order numerical scheme for the hyperbolic conservation law.

6.1 Buckley-Leverett Flux with Dispersion

We begin by computing solutions of Riemann problems using a continuous-in-time, discrete-in-space numerical scheme for the Buckley-Leverett-Dispersive (BLD) model (5.6). The mesh spacing in x is denoted by h. If the solution in $u(x,t)$, then $u_j(t)$ denotes the approximation to $u(jh,t)$ in the numerical method. Our scheme is

$$\begin{aligned} du_j/dt + (g_{j+1/2} - g_{j-1/2})/h = \theta(\epsilon/h^2)(u_{j+1} - 2u_j + u_{j-1}) \\ -(1-\theta)(\epsilon^2/2h^3)(u_{j+2} - 2u_{j+1} + 2u_{j-1} - u_{j-2}), \end{aligned} \tag{6.1}$$

$$\text{where} \qquad g_{j+1/2} = (-f(u_{j+2}) + 7f(u_{j+1}) + 7f(u_j) - f(u_{j-1}))/12,$$

and $f(u_j)$ is the Buckley-Leverett (BL) flux given by (5.8). The parameters $\epsilon > 0$, and $\theta \in [0,1]$ retain their roles from the partial differential equation (5.6).

This non-standard choice for the numerical flux, $g_{j+1/2}$, has the property that

$$(g_{j+1/2} - g_{j-1/2})/h = \partial_x f(u) + O(h^3). \tag{6.2}$$

The numerical scheme (6.1) has the modified equation

$$\partial_t u + \partial_x f(u) = \theta\epsilon\partial_{xx} u - (1-\theta)\epsilon^2\partial_{xxx} u + O(h^3) + O(\epsilon h^2), \tag{6.3}$$

where the error of order ϵh^2 comes from the diffusive term; the discretization of u_{xxx}, gives a smaller error of $O(\epsilon^2 h^2)$. Since we want the scheme (6.1) to approximate a continuous equation, we take the mesh size small enough that it satisfies $h \ll \epsilon \ll 1$. Thus, both of the leading-order error terms are $o(\epsilon^3)$.

In [5] it was shown that a numerical scheme whose modified equation best approximated the *modified Korteweg-de Vries Burgers* (mKdVB) equation, i.e., equation (5.3) with $f(u) = u^3$, gave numerical results which most closely reproduced its known traveling wave solution, derived in [7]. It was also shown in [5], that the computed undercompressive shocks were sensitive to the following quantities: ratio of diffusion to dispersion, represented here by θ, the ratio of diffusion to mesh size, ϵ/h, and the shock strength. In the "good" case of the BLD, the shock strength is bounded by one; for such shock strengths, the scheme (6.1) in [5] had excellent agreement with the analytic solution of the mKdVB equation. As in [5], we also take $\epsilon/h = 4$ in this section.

As in previous sections, we focus on Riemann initial data:

$$u_j(0) = \begin{cases} u_L, & j \le 0, \\ u_R, & j > 0. \end{cases} \tag{6.4}$$

The interval over which the solutions are computed is taken sufficiently large — usually 4000 gridpoints, with $h = 0.0025$, and the run times are limited, so that a region at each end of the computational domain remains in its initial state.

The first set of calculations demonstrate each of the four cases, listed in Section 5, as u_L is varied. In each of Figures 6.1a – 6.1d, we plot the profiles u_j versus jh, at a given time $t_0 > 0$, for a fixed u_L and several choices for u_R, selected to illustrate profiles corresponding to the various intervals shown in Figures 2 – 5. For clarity of presentation, we only plot cases with $u_R > u_I$, as the behavior is identical (and classical) in all four cases, when $u_R \le u_I$.

For each value of the BL flux parameter, a, the dissipation/dispersion parameter, θ, is chosen to lie in the "good" region of Figure 8; i.e., so that Assumption *I* holds. The parameters a and θ are further chosen so that they give rise to profiles which clearly illustrate cases from Section 5.

Once a and θ are specified, we find u_1^- by setting $u_L = 0$ and $u_R = 1$, then running the code. The result, in the good case, is a rarefaction from $u_L = 0$ to $u = u_1^- \in (0,1)$, followed by an undercompressive shock to $u_R = 1$. The intermediate state, u_1^-, is well resolved and can be read off quite accurately. From this value of u_1^-, we find $\bar{u}_1$ via

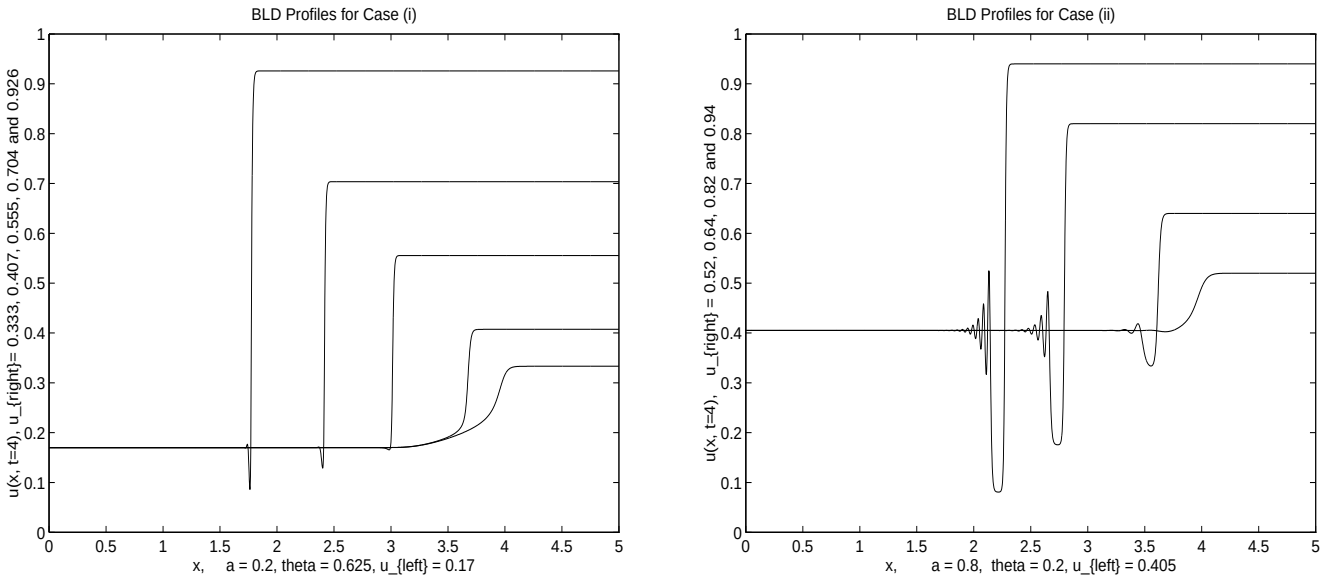

Figure 6.1a: Case (i), left; Figure 6.1b: Case (ii), right.

Newton's method, solving for the middle intersection of the chord from (u_1^-, f_1^-) to $(u, f) = (1, 1)$, with the graph of $f(u)$.

Case (i): The profiles are plotted over $0 \leq x \leq 5$, at $t_0 = 4$, for $a = 0.2$ and $\theta = 0.625$. With this choice of a, we have $\theta^*(a) \approx 0.58$, so that we are in the good case, while the inflection point is at $u_I = 0.2591$. We find that $\bar{u}_1 = 0.1459$, and choose $u_L = 0.17 \in (\bar{u}_1, u_I)$. The result, in Figure 6.1a, is the classical picture of Figure 1: when $u_R = 0.333$ and 0.407, we see a rarefaction-shock (RS), while for larger values of $u_R : 0.555, 0.704$ and 0.906, the solution is merely a single Lax shock. Note that there is some overshoot in the two largest values of u_R; they are still single shocks, in contrast to the pairs of shocks shown in Figure 6.1b, where for large u_R the oscillations in the first shock are clearer.

Case (ii): For $a = 0.8$ and $\theta = 0.2 > \theta^*(a) \approx 0.11$. Now $u_I = 0.4629$, $\bar{u}_1 = 0.4240$, and $u_1^- = 0.0355$. Recall from Figures 3 and 4 that the distinction between Case (ii) and Case (iii) behavior concerns whether or not $u_L > u^*$. Since an accurate value for u^* is difficult to obtain numerically, we simply choose u_L close to, but less than $\bar{u}_1$. For the choice $u_L = 0.405$, we observe Case (ii) behavior: The solution changes from RS to S (Lax shock), then to SΣ, as u_R is increased. We illustrate this with $u_R = 0.52$ (RS), $u_R = 0.64$ (S), and $u_R = 0.82, 0.94$ (both SΣ); the SΣ solution persists until $u_R = 1$.

Case (iii): We now reduce u_L significantly, to 0.2315, while retaining the values of a, θ from Case (ii), so as to illustrate the third case. In Figure 6.1c, we observe in succession, RS ($u_R = 0.57$), RΣ ($u_R = 0.678$), and SΣ ($u_R = 0.785$ and 1). This picture matches

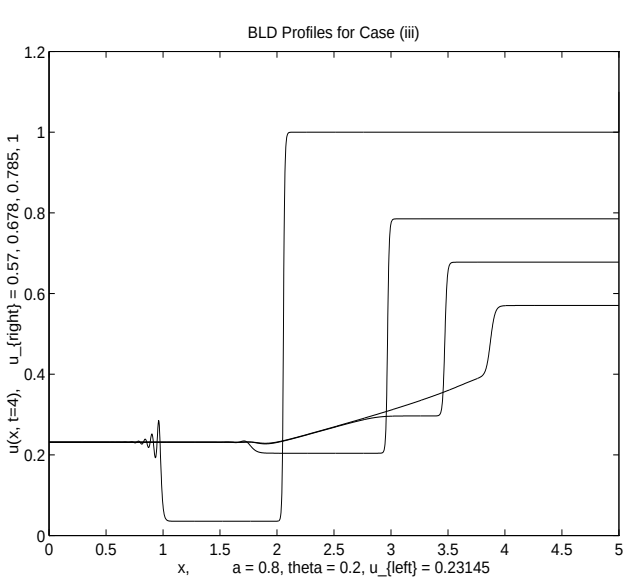

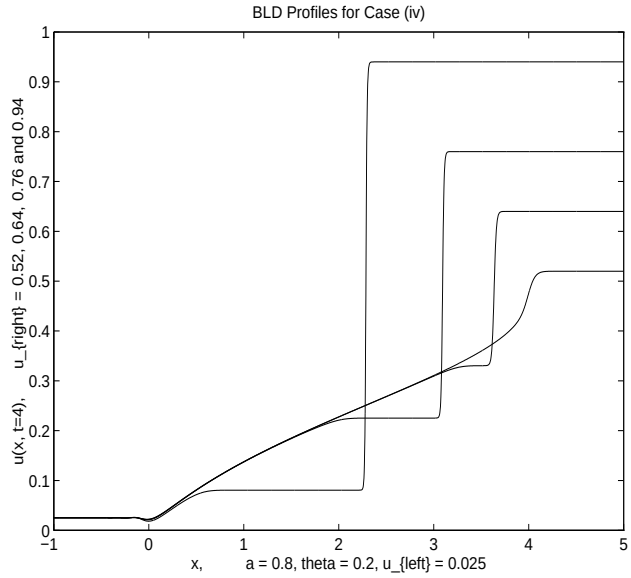

Figure 8c: Case (iii), left; Figure 8d: Case (iv), right.

that of Figure 4.

Case (iv): Retaining $a = 0.8$ and $\theta = 0.2$, as in the two previous plots, we further reduce the left-hand state, so that $u_L = 0.025 < u_1^-$. Our results are consistent with a single transition from RS to RΣ, as u_R is increased: we observe RS at $u_R = 0.52$, and RΣ for $u_R = 0.64$, 0.76 and 0.94, as shown in Figure 6.1d. The slight dip in the computed solutions, occurring near $x = 0$, appears to be a numerical artifact.

Next, in Figure 10, we take $a = 0.5$, $u_L = 0$, and $u_R = 1$, and examine the dependence of the profiles on θ. According to the theory, a solution will stray outside the physical interval, $0 \le u \le 1$, for $\theta < \theta^*(a)$; be an undercompressive shock at $\theta = \theta^*(a)$, and have a rarefaction to u_1^-, followed by an undercompressive shock to $u_R = 1$, for $\theta > \theta^*(a)$. In the case $\theta < \theta^*(a)$, we extend the flux function outside the unit interval, *using the same formula* (5.8). Notice that for $\theta = 0.06, 0.16$ and 0.26, the graphs dip below $u_L = 0$, and their initial shocks (together with oscillations, in the $\theta = 0.06$ case) propagate to the *left*. The critical value is $\theta^*(a) \approx 0.31$, and as expected, we see physical RΣ solutions when $\theta = 0.36$ and 0.46.

6.2 Further Numerical Results

Having demonstrated the structure of solutions of the Riemann problem for the BL flux, we now investigate numerically some fluxes which extend the analysis presented thus far. In particular, we study the Riemann problem for arbitrary initial data, in an exotic,

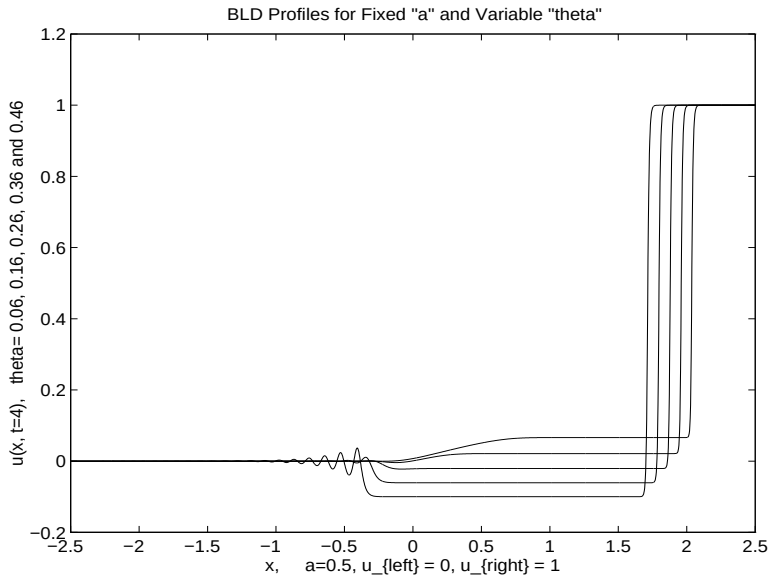

Figure 10: Profiles of the BLD for several values of θ.

bi-asymptotic flux. Our purpose is to draw attention to anomalous behavior, which can creep into the solution. We also study the Riemann problem for $u_L, u_R \in [0,1]$, with a second-order scheme, due to Lax and Wendroff [9]; for the purely hyperbolic Buckley-Leverett equation, this scheme exhibits behavior which is very similar to that of the BLD.

We begin with a nonconvex flux having a single inflection point, but with two different asymptotic slopes as $u \to \pm\infty$. Specifically, we consider

$$f(u) = \begin{cases} \tanh u, & u \geq -1, \\ a\sqrt{u^2 - 1/2} + bu + c, & u < -1, \end{cases} \tag{6.5}$$

where

$$a = -\sqrt{2}\,\mathrm{sech}^2 1 \tanh 1, \quad b = \mathrm{sech}^2 1(1 - 2\tanh 1), \quad c = \mathrm{sech}^2 1(1 - \tanh 1) - \tanh 1,$$

and where the form of the partial differential equation is still that of (5.6), including the sign of the dispersion. The flux (6.5), which we insert in scheme (6.1), has an inflection point at $u = 0$, is a C^1 function of u, and is asymptotic to the (flat) line $u = 1$, as $u \to \infty$, while tending to the line with slope $b - a \approx 0.2326$, as $u \to -\infty$. We plot the flux (6.5) in Figure 11a.

As in the BLD case, we take $u_L < u_I = 0$, and vary u_R. The behavior is similar to that of the BLD, except when u_R is large. There is now a maximum value of u_R, such that a SΣ connection exists from u_L to u_R. Let u_M, with $u_M < u_L < 0$, be the

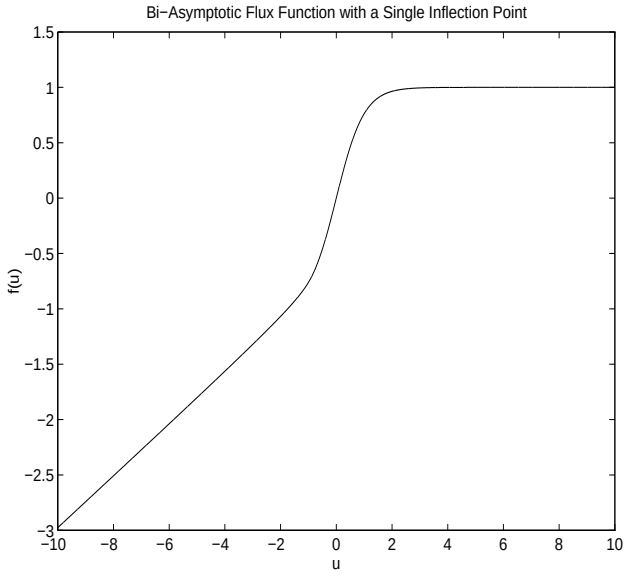

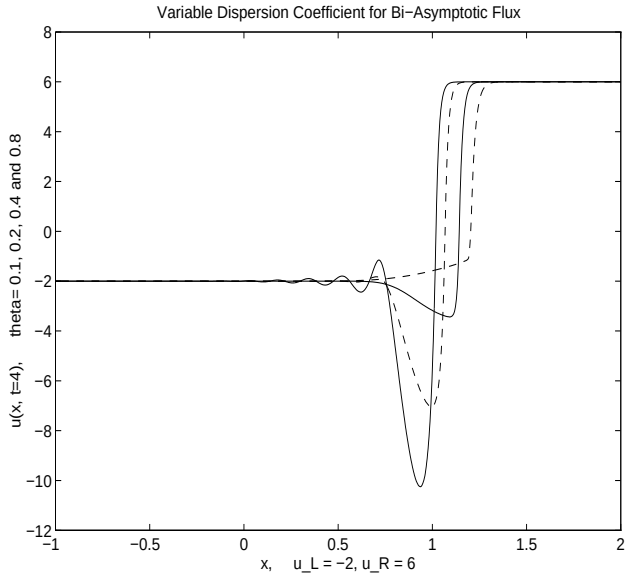

Figure 11a: Bi-asymptotic flux (left); Figure 11b: profiles for several values of θ .

intermediate state following the Lax shock. The maximal right-hand state, denoted by $u_{\max}$, arises because the minimum asymptotic speed of the Lax shock — and hence of the undercompressive shock, as well, is $b-a$. The limiting case occurs when both shocks have this speed, and $u_M \to -\infty$. For $u_L = -2$, as in Figures 11b – 11d, $u_{\max} = 6.573$, determined by where the line through $(u_L, f(u_L))$, with slope $b-a$, crosses the graph of $f(u)$. As long as the Lax shock from u_L to u_M is admissible — which will be true for sufficiently large θ — it can be used to join u_L to $u_R > u_{\max}$; otherwise, it is not clear how, or even if the two states connect analytically. Numerically, in Figures 11c and 11d, we observe a sort of "oscillatory shock", when θ is small.

In Figure 11b, we plot profiles with $u_R = 6$, just below $u_{\max}$, and increase θ (decreasing dispersion!) from zero to one. For $\theta = 0.8$, the solution is clearly RS, while for smaller θ values, the solution has the appearance of an SΣ solution, in which the two shock speeds are nearly equal.

In Figures 11c and 11d, we plot solution profiles for several choices of u_R. The curves in Figure 11c progress from RΣ, when $u_R = 0.5$ and 1.5, to SΣ when $u_R = 2.5$ (the middle curve). The two larger values of u_R also have SΣ-like structure, but the intermediate state is not well-defined. The top curve in Figure 11c, $u_R = 4.5$, becomes the bottom curve in Figure 11d, where the run time has been doubled, to $t = 4$. As u_R is further increased, the solutions become more oscillatory; the two largest values of u_R exceed $u_{\max}$, and it is not clear what types of shock these solutions contain.

Second-order accurate numerical schemes have truncation errors with dispersive terms of $O(h^2)$, but no dissipative terms of $O(h)$. Consequently, they do not fall into the class

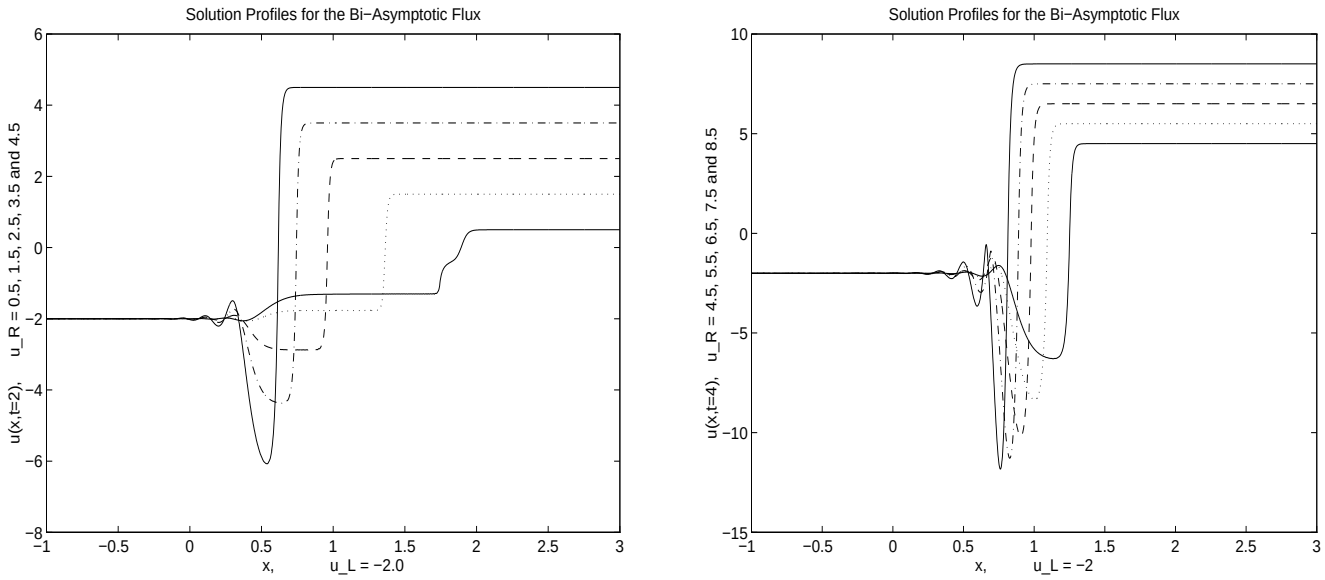

Figure 11c: Profiles for small values of u_R, left; Figure 11d: profiles for large u_R.

of partial differential equations we study here, all of which contain a diffusive term of $O(\epsilon)$ and a dispersive term of $O(\epsilon^2)$. The second-order numerical schemes — of which the Lax-Wendroff (LW) scheme is the archetypal example — do, nevertheless, contain both dissipative and dispersive mechanisms, which can lead them to produce undercompressive shocks.

Whether or not a given second-order scheme develops undercompressive shocks is connected with the sign of the dispersion in its modified equation; see [4]. For LW with the Buckley-Leverett flux, we observe qualitatively similar behavior to that seen with scheme (6.1) for BLD. We note that the second-order Beam-Warming scheme, for which the truncation error has dispersion with the opposite sign, gives rise to only Lax shocks.

To illustrate a second-order scheme that produces undercompressive shocks, we use the two-step Richtmyer version [**?**] of Lax-Wendroff:

$$\begin{aligned} u_j^{n+1} &= u_j^n - \lambda \left(f(\tilde{u}_{j+1/2}) - f(\tilde{u}_{j-1/2}) \right), \\ \tilde{u}_{j+1/2} &= (u_j^n + u_{j+1}^n)/2 - (\lambda/2) \left(f(u_{j+1}^n) - f(u_j^n) \right), \end{aligned} \tag{6.6}$$

where u_j^n approximates the solution, $u(j\Delta x, n\Delta t)$, of the hyperbolic Buckley-Leverett equation, with Δx and Δt the spatial and temporal grid-sizes, respectively. The parameter $\lambda = \Delta t/\Delta x$ must satisfy the CFL condition, $\lambda |f'(u_j^n)| < 1$, for all u_j^n. Also, the flux function, $f(u)$, was taken to be the BL flux (5.8), with the stipulation that if $u \notin [0,1]$, the function is extended using the same formula.

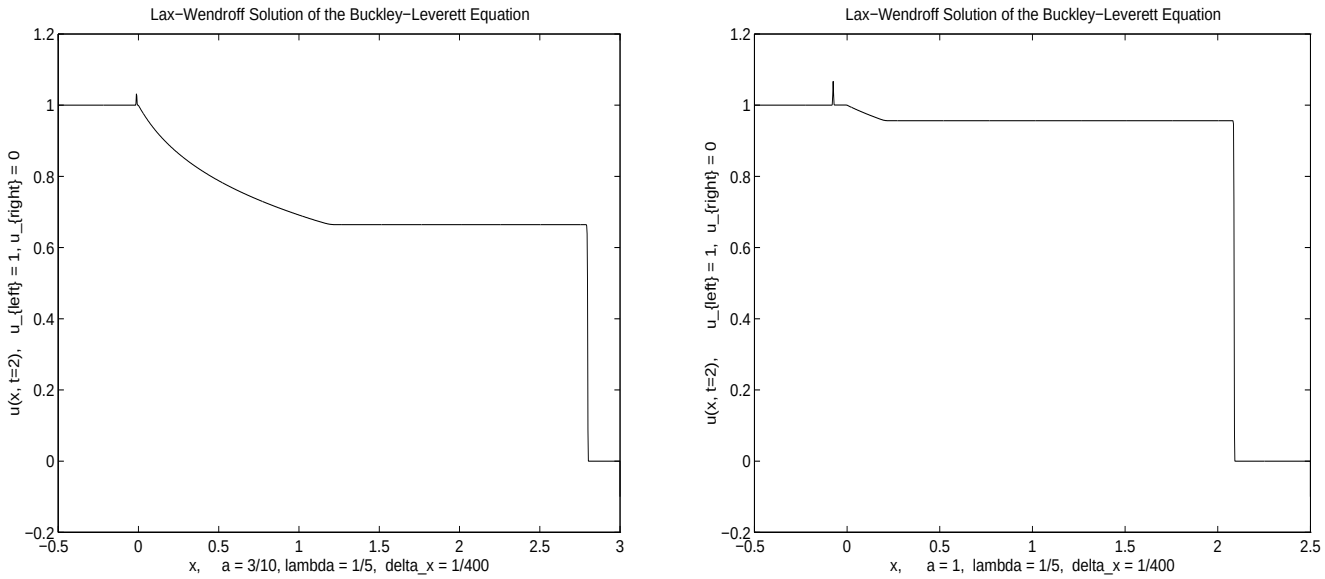

Figure 12a: Lax-Wendroff solution for $a = 0.3$, *(left); Figure 12b:* $a = 1$.

In Figures 12a – d, we plot the numerical solutions of (6.6) for Riemann data and four choices of a. While there is no explicit "θ" for LW, it appears that there is an *effective* value of θ, attained when $\lambda, \Delta x$, and (u_L, u_R) are fixed. Here we take $u_L = 1$ and $u_R = 0$, so that once the solutions lose monotonicity, they leave the physical domain.

From our experience with BLD, we expect that for $a < 1$, there will always be a connection from $u_L = 1$ to $u_R = 0$ — it is the other direction which is problematic — and, indeed, we observe in Figure 12a, with $a = 3/10$, and in Figure 12b, $a = 1$, that (except for a small pulse near $x = 0$) the solutions are RΣ and stay within $[0, 1]$.

Next, we increase $a > 1$, for which the BLD yields unphysical solutions if θ is too small. In Figure 12c, we took $a = 4$, and we see that the solution now has a shock from $u_L = 1$ to $u_M = 1.18$. A more bizarre picture (Figure 12d) emerges for $a = 20$, where the solution contains three shocks, with two intermediate states — both greater than one. In this case, an additional inflection point for $f(u)$ (extended to $u > 1$) has likely influenced the solution.

References

[1] M.B. Allen III, G.A. Behie and J.A. Trangenstein, *Multiphase Flow in Porous Media: Mechanics, Mathematics and Numerics,* Springer Verlag, 1988.

[2] A.V. Azevedo, D. Marchesin, B. Plohr and K. Zumbrun, "Bifurcation of nonclassical viscous shock profiles from the constant state" (1997), preprint.

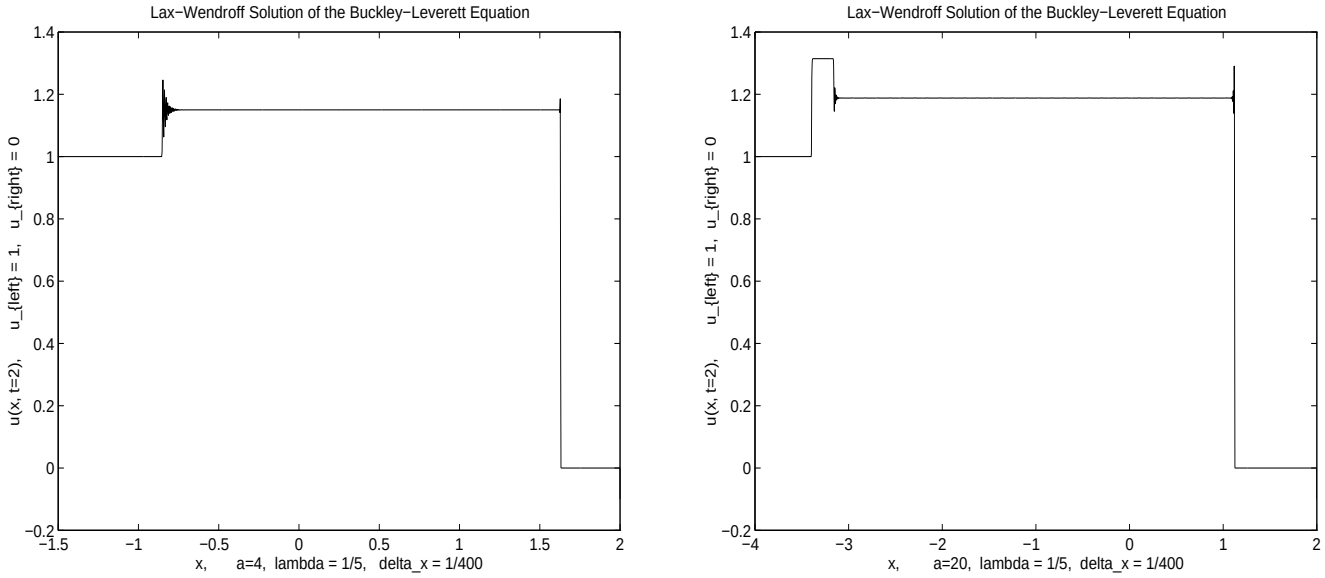

Figure 12c: $a = 4$, (left); Figure 12d: $a = 20$ (right).

[3] J. Guckenheimer and P. Holmes, *Nonlinear Oscillations, Dynamical Systems, and Bifurcations of Vector Fields,* Springer–Verlag, 1983.

[4] B.T. Hayes and P.G. LeFloch, "Nonclassical shock waves: scalar conservation laws", *Arch. Rat. Mech. Anal.*, to appear.

[5] B.T. Hayes and P.G. LeFLoch, "Nonclassical shock waves and kinetic relations: finite difference schemes", *SIAM J. Num Analysis*, accepted for publication.

[6] E. Isaacson, D. Marchesin and B. Plohr, "Transitional waves for conservation laws", *SIAM J. Math. Anal.* **21** (1990), 837–866.

[7] D. Jacobs, W. McKinney and M. Shearer, "Travelling wave solutions of the modified Korteweg-deVries-Burgers equation", *J. Differential Equations* **116** (1995), 448–467.

[8] P.D. Lax, "Hyperbolic systems of conservation laws II", *Comm. Pure Appl. Math.* **10** (1957), 537–566.

[9] P.D. Lax and B. Wendroff, "Systems of Conservation Laws", *Comm. Pure Appl. Math.* **13** (1960), 217–237.

[10] O. Oleinik, "Uniqueness and stability of the generalized solution of the Cauchy problem for a quasilinear equation", *Usp. Mat. Nauk.* **14** (1959), 165–170; English transl. in *Amer. Math. Soc. Transl., Ser 2* **33** (1964), 285–290.

[11] Plohr and Zumbrun paper...?

[12] S. Schecter, Simultaneous equilibrium and heteroclinic bifurcation of planar vector fields via the Melnikov integral. *Nonlinearity* **3** (1990), 79–99.

[13] M. Shearer and Y. Yang, The Riemann problem for a system of conservation laws of mixed type with a cubic nonlinearity. *Proc. A, Royal Soc. Edinburgh* **125A** (1995), 675–699.

[14] M. Slemrod, Admissibility criteria for propagating phase boundaries in a van der Waals fluid. *Arch. Rat. Mech. Anal.,* **81** (1983), 301-315.

[15] C.C. Wu, New theory of MHD shock waves. *Viscous Profiles and Numerical Methods for Shock Waves* (ed. M. Shearer). SIAM 1991.